



Magnesium isotope fractionation by chemical diffusion in natural settings and in laboratory analogues

Rahul Chopra^a, Frank M. Richter^{a,*}, E. Bruce Watson^b, Christian R. Scullard^a

^a *The University of Chicago, Department of the Geophysical Sciences, 5734 South Ellis Avenue, Chicago, IL 60637, United States*

^b *Rensselaer Polytechnic Institute, Department of Earth & Environmental Sciences, Troy, NY 12180, United States*

Received 11 November 2010; accepted in revised form 29 March 2012

Abstract

Laboratory experiments are used to document isotopic fractionation of magnesium by chemical diffusion in a silicate melt and the results compared to the magnesium isotopic composition across contacts between igneous rocks of different composition in natural settings. The natural samples are from transects from felsic to mafic rocks at Vinal Cove in the Vinalhaven Intrusive Complex, Maine and from the Aztec Wash pluton in Nevada. Two laboratory diffusion couples made by juxtaposing melts made from powders of the felsic and mafic compositions sampled at Vinal Cove were annealed at about 1500 °C for 22.5 and 10 h, respectively. The transport of magnesium in the diffusion couples resulted in easily measured magnesium isotopic fractionations at the interface ($\delta^{26}\text{Mg} \sim 1.5\text{‰}$). These isotopic fractionations provide a distinctive isotopic “fingerprint” that we use to determine whether chemical gradients in natural settings where melts of different composition were juxtaposed were due to chemical diffusion. The magnesium isotopic fractionation along one profile at Vinal Cove is exactly what one would expect based on the fractionations found in the laboratory experiments. This is an important result in that it shows that the isotope fractionation by chemical diffusion found in highly controlled laboratory experiments can be found in a natural setting. This correspondence implies that chemical diffusion was the dominant process responsible for the transport of magnesium across this particular contact at Vinal Cove. A second Vinal Cove profile has a very similar gradient in magnesium concentration but with significantly less magnesium isotopic fractionation than expected. This suggests that mass transport at this location was only partly by diffusion and that some other mass transport mechanism such as mechanical mixing must have also played a role. The magnesium isotopic composition of samples from Aztec Wash shows no resolvable isotopic fractionation across the contact between the mafic and felsic rocks. The different degrees of magnesium isotopic fractionation associated with otherwise similar composition gradients in natural settings show that kinetic isotope fractionations provide a key discriminator for establishing whether or not molecular diffusion was the process responsible for an observed elemental gradient. In the one case of a contact at Vinal Cove where we are confident that the magnesium elemental and isotopic gradients were produced by diffusion, we deduced a cooling rate of about 1.5 °C per day.

© 2012 Elsevier Ltd. All rights reserved.

1. INTRODUCTION

There is ample evidence from petrologic and geochemical field studies that magmas of diverse compositions have coexisted in the Earth's crust. We will show that under favorable conditions stable isotope measurements provide

important information regarding the mass transport processes that operated at the interface where the magmas interacted. We use laboratory diffusion couples to document magnesium isotopic fractionations in the chemical diffusion boundary between silicate melts of different composition. The laboratory results are then compared to isotopic fractionations in natural settings where mafic and felsic compositions were juxtaposed. A key concept for the present study is that the only processes that change the chemical concentration of a non-radiogenic element

* Corresponding author.

E-mail address: richter@geosci.uchicago.edu (F.M. Richter).

or isotope in a finite volume of melt are diffusion and/or advection as defined by first and second term on the right hand side of the standard conservation equation $\partial\rho/\partial t = \nabla(D\nabla\rho) + \tilde{u} \bullet \nabla\rho$ where ρ is the molar density of an element or isotope, D is the effective binary diffusion coefficient, and \tilde{u} is the velocity vector defined by the deformation field. Advection involves the physical exchange of material in a finite parcel with its surroundings by such processes as mechanical mixing of two liquids or fractional crystallization and crystal-melt separation. Mixing can alter the isotopic composition only if there are preexisting isotopic gradients in the system while crystal separation will affect the isotopic composition only if there is significant equilibrium isotope fractionation between minerals and melt. Chemical diffusion is distinctive in that it can create isotopic gradients based on the mass dependence of the diffusion coefficients. Recent laboratory experiments have shown that chemical diffusion in silicate melts can fractionate the isotopes of major elements such as calcium (Richter et al., 1999, 2003), magnesium (Richter et al., 2008), and iron (Richter et al., 2009) to a degree that is easily measured. As noted above, mixing can affect the isotopic composition of a given parcel if the parcel and its surroundings have different isotopic composition, but in the case of magnesium this is not likely to be important because there is very little if any isotopic difference between the various igneous rock types (see Table 1). Equilibrium isotope fractionations between minerals and melt are sufficiently small at magmatic temperatures (see Teng et al., 2007) that they are not important in terms of our present study. The key issue we address is not whether chemical diffusion takes place at the interface between magmas of different composition, because it must to some degree, but rather how stable isotope fractionations can be used to determine the relative importance of transport by diffusion compared to advection in producing observed elemental gradients in natural settings.

The chemical composition and magnesium isotope ratios of rock samples from two locations – Vinal Cove in the Vinalhaven Intrusive Complex, Maine and the Aztec Wash pluton, Nevada – were measured to find regions of chemical gradients between contemporaneous mafic and felsic magmas and to determine whether the magnesium isotopes are fractionated across these gradients. Two experimental diffusion couples were made by juxtaposing mafic and felsic composition powders from the rocks at Vinal Cove to calibrate the degree of magnesium isotopic fractionation associated with magnesium diffusion. The degree of correspondence between the magnesium isotopic fractionations found in the laboratory experiments and those from the natural settings are then used to provide a way of determining the dominant transport mechanism responsible for the chemical exchanges across mafic-felsic contacts.

Previous experimental studies by Richter et al. (2003, 2008, 2009) used rhyolite-basalt diffusion couples to document isotopic fractionations of major elements including ^{26}Mg from ^{24}Mg by approximately 7‰ for a concentration ratio of MgO of ~ 10 . The permil notation used for isotopic fractionations is defined as $\delta^n X(\%) \equiv 1000 \times \left[\frac{(^n X/^m X)_{\text{sample}}}{(^n X/^m X)_{\text{standard}}} - 1 \right]$ where $^n X$ and $^m X$ are isotopes of element

X. The magnesium isotopic standard is Dead Sea Magnesium DSM3 (Galy et al., 2003). In the case of laboratory diffusion couples one has to take into account the possibility of significant isotopic fractionations due to temperature differences (i.e., thermal diffusion). Richter et al. (2008) showed that the isotopes of magnesium become enriched at the cold end of molten basalt by $\delta^{26}\text{Mg} \sim 7\%$ per 100 °C temperature difference. In a natural setting temperature gradients will dissipate much faster than chemistry can diffuse for a significant distance and so the kinetic isotope fractionations will be effectively due only to the mass dependence of the chemical diffusion coefficients D of isotopes i and j of mass m_i and m_j . This mass dependence is commonly parameterized by a relationship of the form $D_i/D_j = (m_j/m_i)^\beta$, where β is an empirical quantity determined by laboratory diffusion experiments. The studies by Richter et al. (2003, 2008, 2009) reported $\beta_{Li} = 0.215$, $\beta_{Ca} = 0.05$, $\beta_{Mg} = 0.05$, and $\beta_{Fe} = 0.03$ for molten rhyolite-basalt. Watkins et al. (2009) recently showed that the chemical composition of the juxtaposed melts can significantly affect the value of the fractionation factor β . Because of this, rather than use previously determined magnesium kinetic fractionation factors, we measured the isotopic fractionation of magnesium in new diffusion experiments where melts made from materials sampled at Vinal Cove were juxtaposed.

Several previous studies interpreted isotopic fractionations in natural settings as having been due to mass transport by diffusion. Lundstrom et al. (2005) found variations in lithium isotopic compositions of about 10‰ across dunite to plagioclase lherzolite transects in the Trinity peridotite, California. They interpreted the low $\delta^7\text{Li}$ in harzburgite adjacent to the dunite as being due to the combined process of alkali diffusion and melt extraction. However, the relationship between the concentration and isotopic composition of lithium that they reported was not what is found in the diffusion experiments reported by Richter et al. (2003). Teng et al. (2006) reported what we believe is the best example of correlated lithium concentration and isotope variations in silicate rocks by measuring lithium concentrations and $^7\text{Li}/^6\text{Li}$ in schists and amphibolites in contact with the Tin Mountain pegmatite in the Black Hills of South Dakota. The country rocks in contact with the lithium-rich pegmatite showed a systematic decrease in lithium concentration with distance from the contact and an associated decrease in $^7\text{Li}/^6\text{Li}$ of almost 30‰. This correlation between the concentration and isotopic fractionation of lithium is very similar, except for the length scale, to the diffusive fractionation of lithium reported by Richter et al. (2003). However, the Richter et al. (2003) experiment involved diffusion in a silicate melt whereas the transport mechanism in the case of the lithium derived from the Tin Mountain pegmatite was very likely grain boundary diffusion.

A distinctive feature of the present study is that it uses parameters derived from laboratory diffusion couples made by juxtaposing materials taken from a natural setting to interpret the magnesium elemental and isotopic data from rocks in that setting. Our emphasis on magnesium is due to it being an especially good choice for documenting diffusive isotope fractionations because it does not vary to any great extent ($\sim \pm 0.2\%$) between the igneous rocks ranging

Table 1

Magnesium isotopic composition in per mil relative to standard DSM-3 of the far-field mafic and felsic porphyry powders used to make experimental diffusion couples, of sample slabs from experimental diffusion couples GBM-1 and GBM-2, and of natural samples from VH4 LP-9 and VH4 LP-7b from Vinal Cove and from PC1 LP9 from Aztec Wash. The distances listed give the relative position of the slab centers and drill hole centers. The magnesium isotopic composition of selected geostandards that were measured for comparison to previously reported values are also listed.

Sample	$\delta^{25}\text{Mg}$ (‰)	$\delta^{26}\text{Mg}$ (‰)	Position (mm)
Far-field mafic	-0.15 ± 0.04	-0.32 ± 0.09	
Far-field felsic	-0.28 ± 0.07	-0.59 ± 0.15	
GBM-1-1 (Mafic End)	0.50 ± 0.03	0.99 ± 0.05	5.85
GBM-1-3	-0.38 ± 0.04	-0.74 ± 0.10	4.05
GBM-1-4	-0.67 ± 0.09	-1.35 ± 0.17	3.15
GBM-1-5	-0.96 ± 0.03	-1.89 ± 0.07	2.25
GBM-1-6	-0.78 ± 0.05	-1.51 ± 0.11	1.35
GBM-1-7 (Felsic End)	-0.35 ± 0.02	-0.69 ± 0.04	0.45
GBM-2-1 (Mafic End)	0.21 ± 0.02	0.41 ± 0.03	5.93
GBM-2-3	-0.02 ± 0.08	-0.03 ± 0.16	4.71
GBM-2-4	-0.27 ± 0.03	-0.54 ± 0.07	3.98
GBM-2-5	-0.40 ± 0.05	-0.78 ± 0.08	3.39
GBM-2-6	-0.60 ± 0.12	-1.13 ± 0.24	2.79
GBM-2-7	-0.69 ± 0.11	-1.34 ± 0.23	2.19
GBM-2-8	-0.89 ± 0.07	-1.76 ± 0.10	1.49
GBM-2-9	-0.62 ± 0.11	-1.23 ± 0.24	0.83
GBM-2-10 (Felsic End)	-0.14 ± 0.11	-0.32 ± 0.20	0.21
VH4 LP-9-1 (Felsic)	-1.19 ± 0.08	-2.30 ± 0.18	1.5
VH4 LP-9-2	-1.61 ± 0.16	-3.13 ± 0.35	2.5
VH4 LP-9-3	-1.49 ± 0.15	-2.91 ± 0.33	3.5
VH4 LP-9-4	-0.48 ± 0.06	-0.92 ± 0.12	4.5
VH4 LP-9-5	-0.39 ± 0.07	-0.80 ± 0.13	5.5
VH4 LP-9-6	-0.27 ± 0.03	-0.54 ± 0.06	6.5
VH4 LP-9-7	-0.12 ± 0.10	-0.25 ± 0.05	7.5
VH4 LP-9-8 (Mafic)	-0.16 ± 0.18	-0.32 ± 0.08	8.5
VH4 LP-7b-2 (Felsic)	-0.37 ± 0.18	-0.76 ± 0.32	1.5
VH4 LP-7b-3	-0.89 ± 0.27	-1.77 ± 0.57	2.5
VH4 LP-7b-4	-0.43 ± 0.29	-0.88 ± 0.58	3.5
VH4 LP-7b-5	-0.47 ± 0.10	-0.91 ± 0.19	4.5
VH4 LP-7b-6	-0.09 ± 0.25	-0.16 ± 0.49	5.5
VH4 LP-7b-7	-0.16 ± 0.25	-0.28 ± 0.54	6.5
VH4 LP-7b-8	-0.08 ± 0.20	-0.17 ± 0.39	7.5
VH4 LP-7b-9	-0.10 ± 0.16	-0.19 ± 0.34	8.5
VH4 LP-7b-10 (Mafic)	-0.17 ± 0.19	-0.32 ± 0.34	9.5
PC1 LP-9-2 (Felsic) $n = 3$	-0.35 ± 0.13	-0.46 ± 0.43	1.5
PC1 LP-9-3	-0.24 ± 0.04	-0.48 ± 0.10	2.5
PC1 LP-9-4	-0.16 ± 0.09	-0.32 ± 0.18	3.5
PC1 LP-9-5	-0.24 ± 0.02	-0.50 ± 0.05	4.5
PC1 LP-9-6	-0.15 ± 0.06	-0.30 ± 0.12	5.5
PC1 LP-9-7	-0.12 ± 0.08	-0.25 ± 0.15	6.5
PC1 LP-9-8 (Mafic)	-0.15 ± 0.08	-0.30 ± 0.15	7.5
BCR-2 (Basalt Geostandard) $n = 134$	-0.13 ± 0.07	-0.26 ± 0.13	
SUNY MORB (Basalt Geostandard) $n = 24$	-0.13 ± 0.05	-0.26 ± 0.09	
AB-293 (Granite Geostandard) $n = 16$	-0.12 ± 0.05	-0.23 ± 0.10	
BHVO-1 (Basalt Geostandard) $n = 15$	-0.14 ± 0.06	-0.28 ± 0.10	
AGV-2 (Andesite Geostandard) $n = 15$	-0.12 ± 0.08	-0.22 ± 0.18	

from basalt to granites. The uniformity in the magnesium isotopic composition has been documented in number of recent studies that measured the magnesium isotopic composition of silicate samples from a broad range of igneous rocks and geostandards (Teng et al., 2007; Handler et al., 2009; Huang et al., 2009; Young et al., 2009; Chakrabarti and Jacobsen, 2010; Teng et al., 2010; Liu et al., 2010; Li et al., 2010). This uniformity in the magnesium isotopic composition is especially relevant for our study in that

advection (i.e., magma mixing) will not produce isotopic variations and thus magnesium isotopic fractionations greater than a few tenths of a permil will be diagnostic of diffusive transport. Magnesium has the added advantage of being a major element that varies in abundance by as much a factor of ten between mafic and felsic igneous rocks, and the larger the concentration contrast the larger the isotopic fractionations will be for a given relative mobility of the magnesium isotopes.

2. FIELD LOCATIONS AND SAMPLES

Elemental and magnesium isotopic compositions were measured across the contact between mafic and felsic rocks from Vinal Cove in the Vinalhaven Intrusive Complex, Maine and from the Aztec Wash pluton in Nevada. The goal was to find chemical composition gradients over a sufficient distance that would allow for magnesium isotopic measurements in the boundary layer.

2.1. Vinal Cove, Vinalhaven Intrusive Complex, Maine

The samples analyzed belong to a felsic porphyry body with coeval gabbro, hybrid rocks, and coarse-grained granite in the Vinal Cove complex of the Silurian Vinalhaven Intrusive Complex in Maine (Fig. 1). The plutonic rocks on Vinalhaven Island belong to the Coastal Maine Magmatic Province consisting of more than 100 bimodal granite-gabbro plutons (Hogan and Sinha, 1989). The geology, field relations, petrogenesis, and the origin and evolution of the Vinalhaven Intrusive Complex have been described by Wiebe et al. (2001, 2004), Hawkins et al. (2002), and Wiebe and Hawkins (2003). The complex consists of three main units: A coarse-grained granite unit, a

gabbro-diorite unit, and a younger fine-grained granite unit. It also contains several bodies of felsic porphyry that occur within the coarse-grained granite. The largest body of porphyry occurs in the Vinal Cove complex.

According to Wiebe et al. (2004), “the rocks of the Vinal Cove complex record events during the waning stages of solidification of the Vinalhaven intrusive complex, when a large mafic dike intruded a small, partially molten, inner portion of the mostly solidified coarse-grained Vinalhaven granite.” The authors argued that the 20–30 cm thick zone of felsic porphyry at locality V2-42, which we sampled, was formed largely by the local thermal rejuvenation of the Vinalhaven granite during the emplacement of the mafic dike.

Fig. 2a shows the outcrop we sampled where the chilled margin of the gabbro is separated from coarse-grained granite by about 20–30 cm of felsic porphyry. This zone of porphyry has an aphanitic matrix with about 20–30% phenocrysts. The phenocrysts are mainly subhedral to anhedral quartz, feldspar and biotite and are often corroded. The porphyry also contains a few small (1–5 mm) quenched mafic droplets. Some alkali feldspars are rimmed by plagioclase. The chilled gabbro is characterized by an aphanitic texture and has a typical mineralogy of feldspar, pyroxene, hornblende, biotite and minor Fe-Ti oxides. Fig. 2b shows a closer view of the irregular contact between the felsic porphyry and the chilled gabbro, and the location of two profiles (LP 7b and LP 9) along which the bulk composition was measured and samples drilled for magnesium isotopic analyses.

2.2. Aztec Wash Pluton, Nevada

The sample from Nevada analyzed in this study belongs to an outcrop of a well-defined contact between mafic and felsic magma at Pipe Canyon in the Aztec Wash pluton located in the central Eldorado Mountains near the southern tip of Nevada. The Aztec Wash pluton is a shallow (4–7 km in depth) pluton of Miocene age (15.7 Ma) that is exposed over an area of approximately 50 km². The geology and petrogenesis of the pluton has been discussed in detail by Falkner et al. (1995), Patrick and Miller (1997), Harper et al. (2004), Miller et al. (2005), and Miller et al. (2011). These studies emphasize complex, open-system histories involving multiple recharge events with mingling and mixing between felsic and mafic magmas in the evolution of the pluton. It underwent a brief episode of extreme extension. The pluton intrudes Proterozoic gneisses, Cretaceous granite, and slightly older Miocene intrusive and extrusive rocks. Northward tilting associated with extension in the mid-Miocene resulted in exposure of a complete vertical cross section of the pluton.

The Aztec Wash pluton can be divided into two distinct, major zones: An upper ‘homogeneous’ granite zone and a lower heterogeneous zone. To a first approximation, the granite zone is chemically and texturally homogeneous. Essential minerals in the granites tend to be unzoned or weakly zoned. The heterogeneous zone of the pluton preserves clear magmatic and geochemical features that provide evidence for an open system history. The dominant

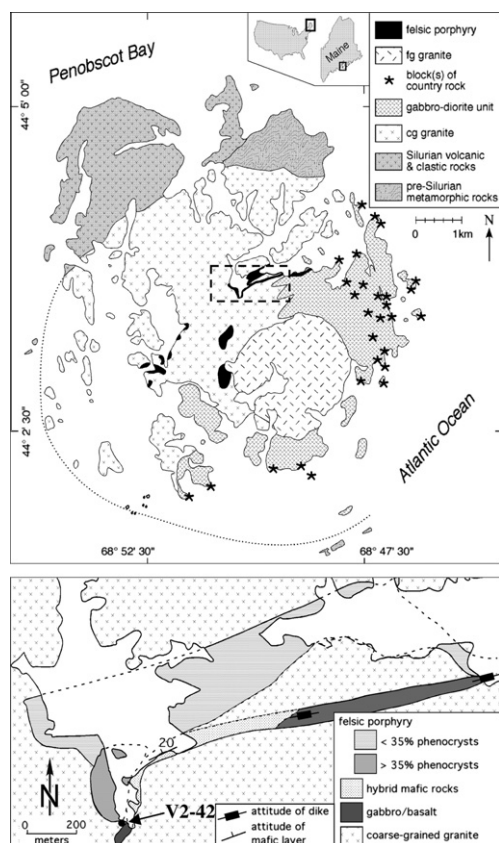


Fig. 1. Top panel shows a geological map of the Vinalhaven intrusion on Vinalhaven Island, Maine. The dash-lined box shows the location of the Vinal Cove complex, which is shown in greater detail in the lower panel. Both maps are based on those given in Wiebe et al. (2004) and the VH4 sample analyzed in this study is from locality V2-42 of Wiebe et al. (2004).

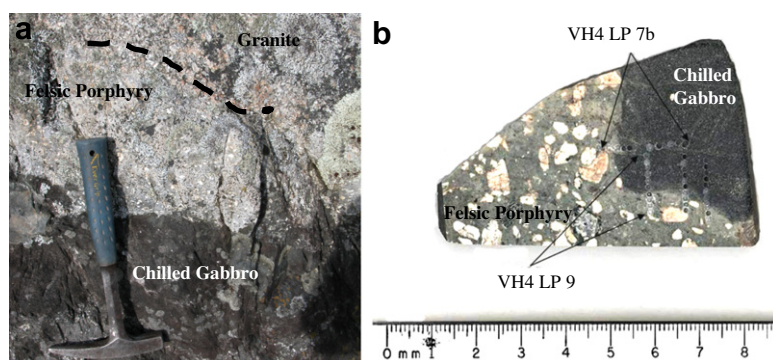


Fig. 2. The picture on the left (a) shows the outcrop with the coarse-grained granite, felsic porphyry and the chilled gabbro that was sampled at Vinal Cove. The contact between the felsic porphyry and the coarse-grained granite is gradational and somewhat obscured by the growth of lichens. The picture on the right (b) shows the contact between the felsic porphyry and chilled gabbro in sample VH4 and the location of the two profiles, VH4 LP7b and VH4 LP9, along which the bulk composition was measured and samples drilled for magnesium isotopic analyses.

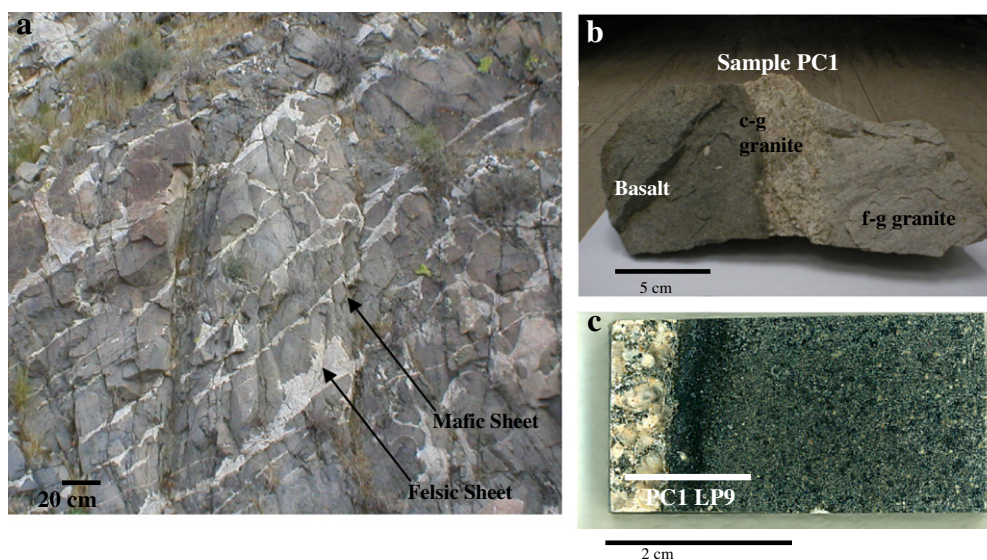


Fig. 3. (a) Alternating mafic and felsic sheets in the heterogeneous zone of the Aztec Wash pluton, Nevada. (b) Picture of sample PC1 from Pipe Canyon in the Aztec Wash Pluton showing the contact between the basalt and coarse-grained granite as well as the contact between coarse-grained granite and fine-grained granite. (c) Closer view of the contact between basalt and coarse-grained granite. Also shown in (c) is the location of profile LP 9 along which the bulk composition was measured and samples drilled for magnesium isotopic analyses.

features within the heterogeneous zone are alternating mafic and felsic sheets (see Fig. 3a). The felsic sheets are mainly quartz monzodiorites that are interpreted as cumulates deposited from a granitic magma (Miller et al., 2005). The mafic sheets typically have chilled, crenulate margins against the felsic sheets on one side, indicating that cooler felsic melt was present in the adjacent sheet when the mafic sheet was emplaced (Miller et al., 2005). Based on the orientations of petrologic indicators such as flame structures and load casts, it is thought that the mafic sheets spread as lava flows on the effective base of the granitic magma chamber, quenching against the cooler substrate of crystals accumulated from the overlying granitic magma (Falkner et al., 1995; Patrick and Miller, 1997; Miller et al., 2005). The heterogeneous zone contains more than 100 mafic sheets, each one thought to represent a mafic recharge event

(Miller et al., 2005). The specific contact sampled for the present study is shown in Figs. 3b and c.

3. EXPERIMENTAL AND ANALYTICAL METHODS

3.1. High-temperature diffusion experiments

The laboratory diffusion couples were constructed using powders of the far-field felsic porphyry and the far-field chilled gabbro from sample VH4 from Vinal Cove, Vinalhaven, Maine. The term far-field is used to denote samples taken sufficiently far from the contact between the felsic porphyry and the gabbro for them not to have been affected by diffusion. Special care was taken to use material from the aphanitic matrix in the felsic porphyry portion of the sample to minimize the effects of large phenocrysts. Diffusion

couples GBM-1 and GBM-2 were made by juxtaposing the far-field felsic and mafic powders in a graphite capsule within a piston cylinder assembly and annealing them at about 1500 °C and 1.45 GPa for 22.5 and 10 h, respectively. The experiments were run at this moderate pressure to avoid forming bubbles, which would generate unwanted motions were they to rise through the melt. The piston cylinder assembly (Fig. 4a) consists of NaCl and Pyrex outer sleeves with MgO filler pieces inside a tubular graphite furnace. The thermocouple is insulated by an alumina tube, which is surrounded by MgO in the upper portion of the assembly while MgO and Al₂O₃ are used as filler pieces in contact with one another in the lower portion of the assembly. The temperature gradients above and below the diffusion couples were determined using a method developed by Watson et al. (2002) where the spinel forming reaction $\text{MgO} + \text{Al}_2\text{O}_3 \rightarrow \text{MgAl}_2\text{O}_4$ is used to monitor the local temperature at a number of places in the assembly. Watson et al. (2002) calibrated the rate at which spinel is formed and presented a general relationship describing the width of the spinel layer as a function of time, temperature, and pressure. Thus, given the duration of an experiment, the pressure and the thickness of the spinel layer that formed at various places where MgO and Al₂O₃ was in contact, the temperature at each such point can be determined. Fig. 4b and c show backscattered images of GBM-1 and GBM-2 samples after quenching and Fig. 4d shows the temperatures determined by the spinel thickness thermometer above and below experiment GBM-1. The inferred temperature distribution within the sample assembly indicates that the molten sample might have varied by more than 20 °C, especially in the more mafic parts. Given that Richter et al. (2008, 2009) showed that thermal diffusion due to temperature gradients in a piston cylinder assembly will measurably fractionate isotopes, the effect of tempera-

ture differences has to be taken into account when modeling the magnesium data from the diffusion couples.

3.2. Major element analysis

The quenched glass from the laboratory diffusion couples and the natural rock samples were cut, polished with silicon carbide polishing compounds, and then coated with a carbon layer for imaging and chemical analysis. Major element concentrations were measured using a JEOL JSM-5800LV scanning electron microscope equipped with an Oxford Link ISIS-300 energy dispersive X-ray microanalysis system. The analysis conditions involved a 15 kV primary beam and the typical precision of such measurements is better than 1% relative. Major element concentration profiles were measured along the length of the diffusion couples GBM-1 and GBM-2 by rastering the beam over a scan area of 70 μm × 50 μm. The distance between analyzed data points was 50 μm. Several major element concentration profiles were measured across the mafic-felsic interfaces of the natural samples VH4 from Vinal Cove and PC1 from Aztec Wash. In the case of sample VH4, major element concentrations were measured at a magnification of 250 that corresponded to a scan area of 600 μm × 400 μm and the distance between analyzed data points was 300 μm. For sample PC1 a magnification of 190 was used, which corresponds to a scan area of 800 μm × 550 μm and the distance between analyzed data points was 500 μm. The magnifications and corresponding scan areas were set so as to minimize the effects of individual mineral grains as much as possible.

After the laboratory and the natural samples had been analyzed for the major element concentrations, selected portions of these were sampled for magnesium isotopic analyses. Diffusion couples GBM-1 and GBM-2 were

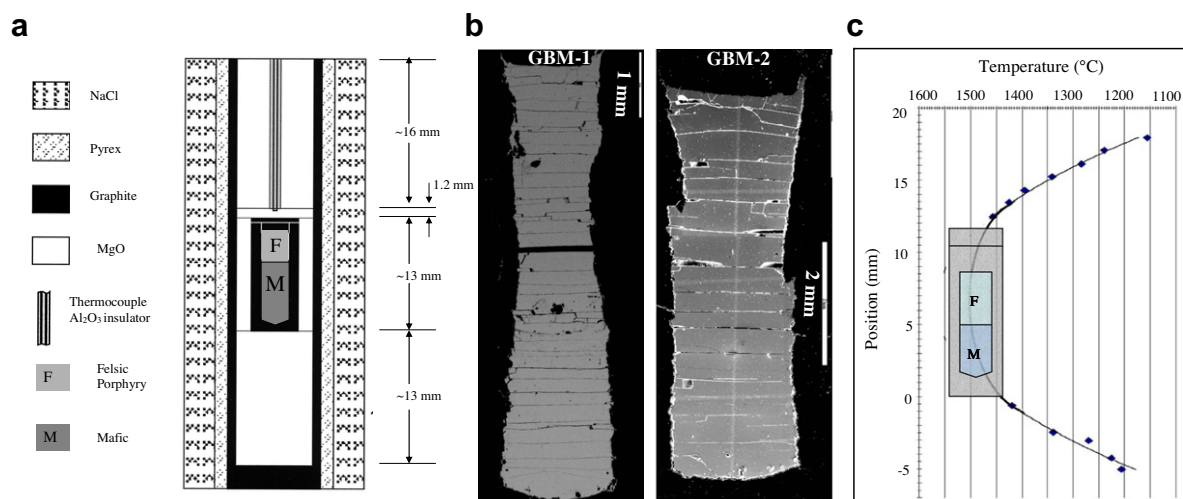


Fig. 4. (a) Pre-compaction dimensions of the piston cylinder assembly used to make diffusion couples GBM-1 and GBM-2. (b) Backscattered electron images of the exposed portion of the quenched glass from samples GBM-1 and GBM-2. Decompression cracks, which are common in glass recovered from piston cylinder experiments, are evident in the run products. (c) The filled diamonds show the places above and below the sample assembly where temperatures were determined using the thickness of the spinel layer that developed where MgO and Al₂O₃ were juxtaposed. The temperature profile is interpolated into the molten sample based on temperatures measured by Watson et al. (2002) for a similar piston cylinder assembly where MgO and Al₂O₃ had been juxtaposed throughout the entire assembly.

sectioned into a series of slabs perpendicular to their long axes of approximate thickness 0.9 mm and 0.5 mm, respectively. In the case of the natural samples, two line profiles in sample VH4 (VH4 LP9 and VH4 LP7b) and one line profile in sample PC1 (PC1 LP9) were chosen for further analyses (see Figs. 2b and 3c). Approximately 1 mm diameter holes were drilled along these profiles to recover sample powders for chemical and isotopic analysis. The samples were drilled using diamond-coated dentist's drill bits. The drill bits were cleaned with acetone in an ultrasonic bath for at least 10 min between uses to ensure that there was negligible cross-contamination of samples due to the drilling process.

3.3. Separation and isotopic analysis of magnesium

Between 1 and 10 mg of the sample powders and slabs were dissolved in a 3:1 mixture of concentrated HF:HNO₃ acids, which after repeated drying down and re-suspension were finally dissolved in 1 N HNO₃ for chromatographic separation. The chemical separation of Mg by cation exchange chromatography was done using ion exchange resin AG50W-X8 (Bio-Rad 200–400 mesh) following the procedure described by Teng et al. (2007). Approximately 1 ml of resin was loaded in an ion exchange column made of quartz glass. One hundred μ l of sample in 1 N HNO₃ was introduced into the column and eluted using 1 N HNO₃. Elution curves for three natural rock samples (two basalt geostandards – SUNY MORB and BCR-2 – and one granite in-house rock standard AB 293) were obtained in order to determine when the magnesium cut was eluted through the columns. The elution curves for all the geostandards sampled at one ml increments showed that the magnesium was completely eluted through the columns in the 7 ml of 1 N HNO₃ from cuts 7 to 13 and that the calcium and aluminum concentration were sufficiently low so that they would not affect the magnesium isotopic measurements.

The magnesium isotopic analyses were performed at the University of Chicago with a Thermo Scientific Neptune MC-ICPMS in the medium resolution mode (see Dauphas et al. 2009 and references therein for a detailed description of the instrument). An enclosed SC-2 sample changer equipped with a ULPA (ultra low particle arrester) filter unit was used together with the Apex-Q + Spiro TMD desolvating inlet system from Elemental Scientific Inc. The Neptune was run with nickel sampler and skimmer cones. The three isotopes of Mg and ²⁷Al were measured simultaneously by multi-collection on the L3, C, H2, and H4 Faraday collectors respectively. The magnesium isotopes were measured as standard–sample sequences acquired in a block consisting of 20 cycles of 8.389 s each. The washout time with 3% HNO₃ rinse between samples and standards was 90 s. The takeup time was 60 s. Before each sequence of analyses, a Mg-free 3% HNO₃ solution was measured under conditions identical to the sample measurements. The ion intensities of this solution were subtracted from all sample/standard measurements. The standard-sample sequences were repeated *n* times (typically *n* = 8). The Mg standard used throughout this study was Dead Sea Magnesium DSM3 (Galy et al. 2003). In a sequence consisting of standard (*i* – 1), sample (*i*), standard (*i* + 1) the magnesium

isotopic composition of the sample is calculated in per mil as

$$\delta\text{Mg}_{\text{sample}(i)} (\%) = 1000 \times \left(\frac{2R_{\text{sample}(i)}}{(R_{\text{std}(i-1)} + R_{\text{std}(i+1)})} - 1 \right)$$

where *R* is the ratio of the magnesium isotopes (e.g., ²⁶Mg/²⁴Mg). The value reported for a given sample is the average of the *n* repeated measurements. δMg values for standards were also computed by considering each standard (*i*) as a sample bracketed by standards (*i* – 1) and (*i* + 1). The dispersion of the δMg values for the standards was used to estimate the instrument uncertainty (σ), which was then used as a measure of the uncertainty of the isotopic composition of the sample in the same sequence (i.e., $\sigma_{\text{sample}} = \sigma_{\text{standard}}$ as discussed by Dauphas et al., 2009). As a further test of the quality of our magnesium isotopic measurements five geostandards were run (Table 1) and the our values are within the stated error of previously reported values by Teng et al. (2007) for SUNY MORB, BCR-2 basalts, by Huang et al. (2009) for BCR-2 and BHVO-1 basalts, and by Teng (personal communication) for AB-293 granite.

The internal precision of the reported $\delta^{26}\text{Mg}$ values is better than $\pm 0.15\%$ (95% confidence interval CI) based on eight repeat runs of the same sample solution during a single analytical session. The external precision of the $\delta^{26}\text{Mg}$ values, based on repeated measurements during the course of this study is $\pm 0.13\%$ (95% CI). The external precision of the $\delta^{26}\text{Mg}$ values, based on repeated analyses of the standard (DSM3) bracketed by the standard (DSM3) performed over the course of this study is better than $\pm 0.10\%$ (95% CI). The generally conservative conclusion based on these various measures of precision and comparisons to published data is that the magnesium isotopic compositions we report have uncertainty of no more than $\pm 0.20\%$ at 95% CI. However, there are a few occasions when instrument stability issues gives rise to uncertainties that are somewhat larger than this, and for this reason we list the uncertainty of each sample's magnesium isotopic composition based on the internal precision of repeated measurements of the purified sample solution.

4. RESULTS

The major element and magnesium isotopic composition of the experimental diffusion couples and the natural samples were measured along traverses perpendicular to interface between the mafic and felsic compositions. The magnesium isotopic compositions are given in Table 1.

4.1. Chemical and magnesium isotopic composition of the experimental samples

The weight percent of major oxide components measured along the length of laboratory diffusion couples GBM-1 and GBM-2 are shown in Fig. 5. The asymmetry of the concentration profiles is due to faster diffusion in the mafic melt than in the felsic one. A subtle but important feature of the concentration profiles of both samples is the non-zero gradient of the concentrations at the mafic end of

the diffusion couple. There can be no mass transport across the ends of the diffusion couple and thus the condition of no mass flux there would seem to require that the concentration gradients go to zero as the boundary is approached. The major element compositions measured along parallel profiles in both samples were found to be indistinguishable thereby establishing that the systems were effectively one-dimensional and that the gradient at the boundary was not balanced by fluxes in other directions. This leaves the effect of a temperature gradient as the most likely explanation of the non-zero gradients at the mafic end of the couples. It is well known that when a temperature difference is imposed across a silicate liquid there will be a mass flux due to the thermal differences, a process that is commonly referred to as Soret diffusion (see *Lesher and Walker, 1986* for experimental examples). The non-zero chemical gradients at the mafic end of the two diffusion couples would not be a violation of the no flux boundary condition if a sufficiently large temperature gradient drives a flux opposite

to the flux due to the chemical gradient. Additional evidence that this is indeed the case is given in a later section based on the magnesium isotopic fractionation at the two ends of the diffusion couples.

The magnesium isotopic composition of slabs cut perpendicular to the long axis of the diffusion couples is shown in *Fig. 6*. The most obvious common feature of the isotopic compositions is the well-resolved negative $\delta^{26}\text{Mg}$ values in the vicinity of the original interface compared to the starting isotopic compositions. The positive $\delta^{26}\text{Mg}$ values, most notably at the mafic end are discussed below as being the result of thermal fractionation of the magnesium isotopes.

4.2. Chemical and isotopic composition of the natural samples

The natural samples from Vinal Cove and from Aztec Wash are made up of distinct mineral phases of various sizes and as a result the compositional data shown in *Fig. 7* are

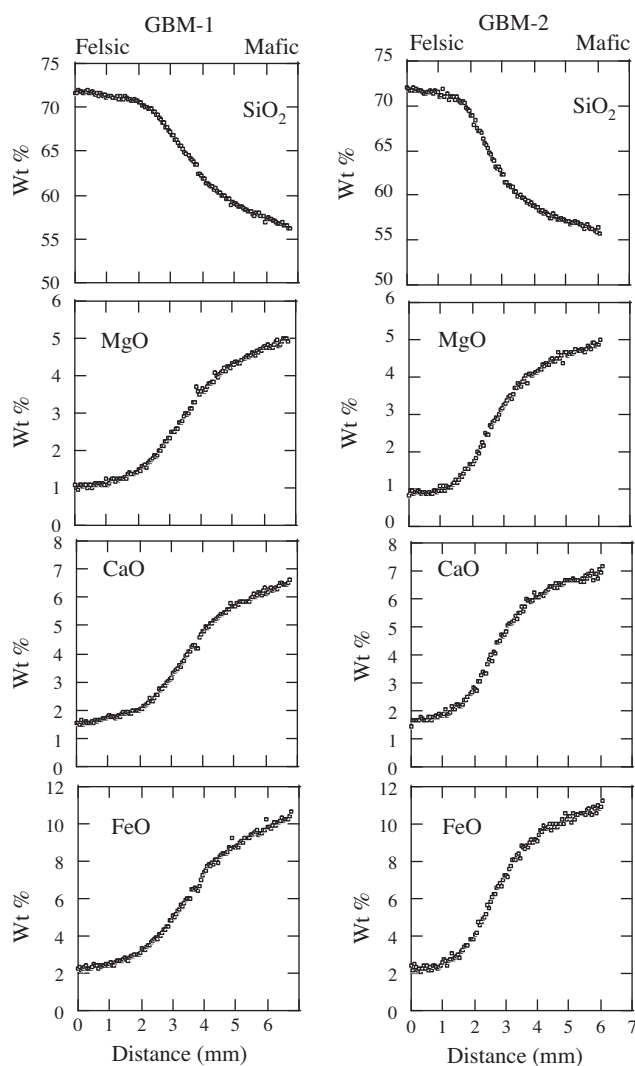


Fig. 5. Concentration profiles of selected major oxides from samples GBM-1 (22.5 h at $T \sim 1500^\circ\text{C}$ and $P = 1.45\text{ GPa}$) and GBM-2 (10 h at $T \sim 1500^\circ\text{C}$ and $P = 1.45\text{ GPa}$). Note that the concentration gradients at the mafic end do not go to zero, which is an indication that thermal diffusion fluxes are balancing the fluxes associated with the composition gradients so as to satisfy the no net flux condition at the boundary.

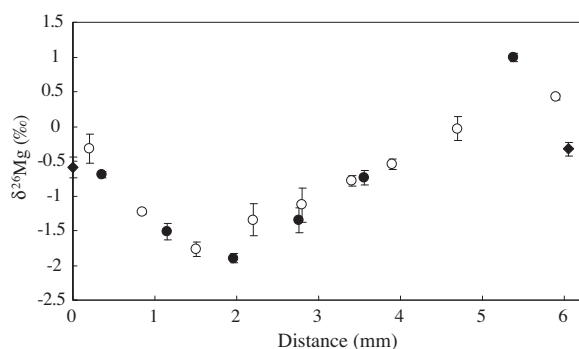


Fig. 6. Magnesium isotopic composition relative to standard DSM-3 of slabs cut at various distances along diffusion couples GBM-1 (black filled circles) and GBM-2 (black unfilled circles) along with the 95% confidence limits. The black diamonds at the edge of the figure show the magnesium isotopic composition of the felsic (on the left) and mafic (on the right) rock powders that were used to make the diffusion couples.

more scattered than what was measured in the glass recovered from the piston cylinder experiments. Despite the scatter, the similar changes in weight percent CaO, MgO, and FeO as a function of distance are indicative of compositional gradients that would seem to suggest diffusive exchange of these oxides from the mafic part to the more felsic part. Fig. 8 shows the magnesium isotopic composition of powder drilled along the same transects where the compositional data was measured. The magnesium isotopic composition of samples taken far from the contact were also measured (shown as stars in Fig. 8) and they are sufficiently similar that isotopic variations in excess of a few tenth of a per mil cannot have been produced by mixing.

5. THERMO-CHEMICAL DIFFUSION

This section begins with an outline of the mathematical formulation used to model the diffusion of elements and isotopes by both chemical and thermal differences. The resulting equations are used to solve several idealized model problems that illustrate how the various properties of the system of interest here affect the elemental and isotopic evolution as a function of time and distance. More specific model calculations are then used to fit the data from the experimental diffusion couples and determine the effective binary diffusion coefficient for magnesium and the relative mobility of the magnesium isotopes. After the kinetic isotope fractionation parameters were determined from the laboratory experiments, model calculations were used to fit the silicon and magnesium concentration data from the natural samples and to calculate the magnesium isotopic fractionation that should be observed if the mass transport in the natural system had been governed the same processes and parameters as in the laboratory experiments.

5.1. Model equations

The mathematical representation of the one-dimensional thermochemical diffusion problem we will use follows from that given in Richter et al. (2008) and in a more concise

fashion in Richter et al. (2009). The conservation equation for an element or isotope i is

$$\frac{\partial \rho_i}{\partial t} = -\frac{\partial J_i}{\partial x}, \quad (1)$$

where ρ_i is the molar density of component i , and J_i is the flux in moles/cm²s. The flux in a one-dimensional system with both concentration and temperatures differences is written as

$$J_i = -\rho(D_i \partial \omega_i / \partial x + D_T^i \omega_i (1 - \omega_i) \partial T / \partial x) \quad (2)$$

where ρ is the bulk molar density of the system, D_i is the effective binary diffusion coefficient (EBDC) of component i , ω_i is the mole fraction of i , D_T^i is the thermal diffusion coefficient, and T is temperature. In specifying the flux by Eq. (2) we have implicitly assumed no flow in the x direction (i.e., $u_x = 0$) and thus the mass flux $u_x \rho \omega_i$ due to advection is not included. Combining Eqs. (1) and (2) results in the following equation for the evolution of the elemental mole fractions.

$$\partial \omega_i / \partial t = \frac{\partial}{\partial x} (D_i \partial \omega_i / \partial x + D_T^i \omega_i (1 - \omega_i) \partial T / \partial x) \quad (3)$$

For isotopes, Eq. (3) is replaced by

$$\partial \omega_i / \partial t = \frac{\partial}{\partial x} (D_i \partial \omega_i / \partial x + D_T^i \omega_i (1 - \omega_e) \partial T / \partial x) \quad (4)$$

where ω_e is the mole fraction of the parent element of the isotopes i . Eq. (4) becomes the equation for the parent element (Eq. (3)) when summed over all the isotopes i . The boundary conditions used in connection with Eqs. (3), (4) are no flux (i.e., $J_i = 0$) at each end of the diffusion couple, or in the case of a natural sample, at a distance sufficiently far from the contact between the different rock types that the calculated diffusion profile is not affected by the boundary conditions. Note that the boundary condition $J_i = 0$ together with Eq. (2) requires that there be a concentration gradient at the boundary if $\partial T / \partial x \neq 0$. The initial conditions used are a step function in the elemental and isotopic concentrations as required by the properties of the juxtaposed melts. The temperature distribution in the piston cylinder assembly is assumed to have been unchanging over the course of the experiment.

Eqs. (3) and (4) are solved numerically with the following parameter specifications. Time in the calculation is measured in nondimensional units L^2/D_o where L is the length of the calculation domain and D_o is the effective binary diffusion coefficient (EBDC) of SiO₂ for a melt with a SiO₂-weight fraction $X_{SiO_2} = 0.52$. The EBDC of the other elements in this reference melt are specified as a ratio relative to D_o . The obvious asymmetry of the laboratory diffusion profiles (Fig. 5) is an indication that the chemical diffusion coefficients are composition dependent. This dependency is modeled in terms of the SiO₂ content using the parameterization.

$$D_{i(SiO_2)} = D_{i(X_{SiO_2}=0.52)} e^{-\alpha_i (X_{SiO_2} - 0.52)} \quad (5)$$

The parameter α_i specifies the degree to which the EBDC of element i changes with the amount of SiO₂ in the melt. The thermal diffusion coefficient is also specified relative

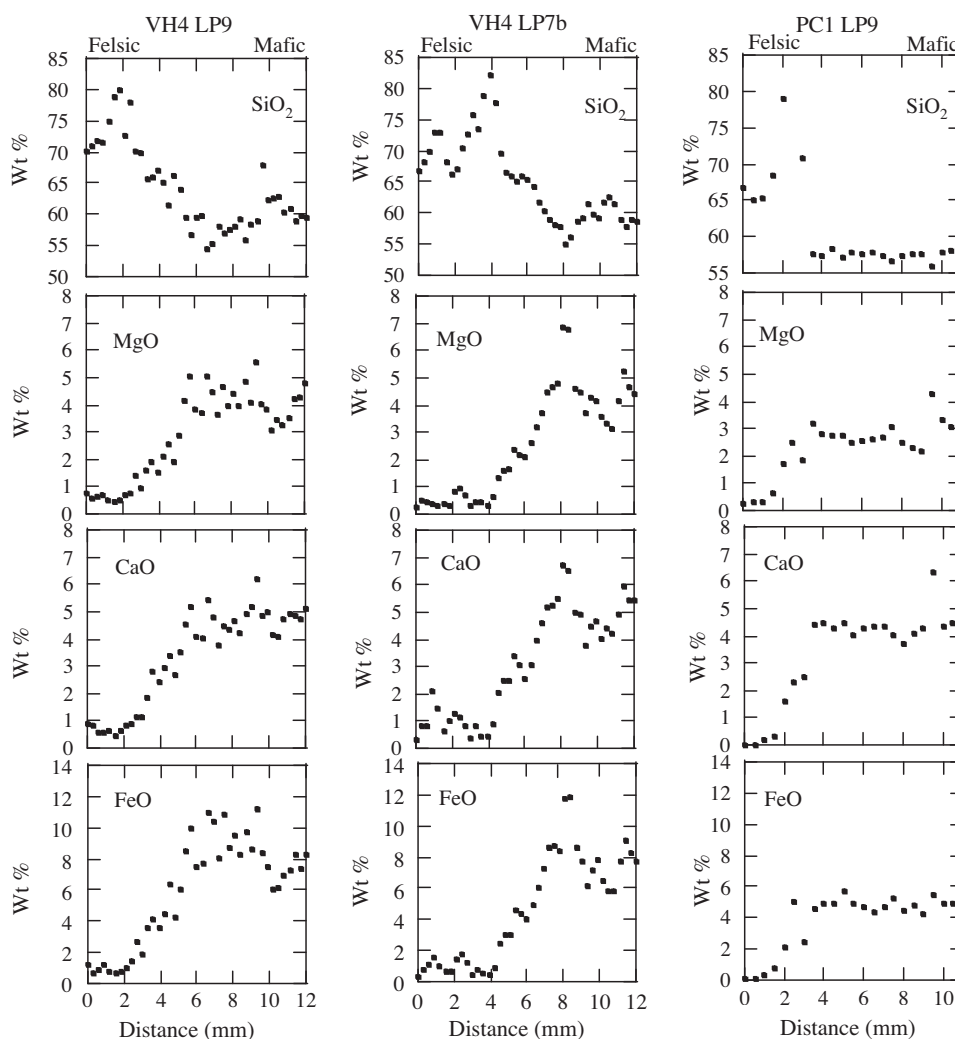


Fig. 7. Selected major element concentration data measured along line profiles 9 (left column) and line profile 7b (center column) in sample VH4 from Vinal Cove, and along line profile 9 in sample PC1 from Aztec Wash (right column).

to D_o by a Soret coefficient $\sigma_i = D_T^i/D_o$ for each component i . When solving Eq. (4) for the isotopic evolution of a system one needs to take into account that both the chemical and thermal diffusion coefficients are mass dependent. These are specified by the parameters β and β_T in $D_i/D_j = (m_j/m_i)^\beta$ and $D_T^i/D_T^j = (m_i/m_j)^{\beta_T}$.

5.2. Thermo-chemical diffusion model calculations for idealized cases

We begin by considering several idealized cases to illustrate how various properties of a chemical diffusion system determine the degree and form of isotopic fractionation. Fig. 9a shows the profile of wt.% SiO_2 as a function of normalized distance x/L , where L is the dimensional size of the domain, at a nondimensional time $t' = L^2/D_{\text{SiO}_2}(X_{\text{SiO}_2=0.52}) = 0.1$. The asymmetry of the SiO_2 profile is due to the dependence of the diffusion coefficient on the SiO_2 content, which is specified in this example by $\alpha = 10$ in Eq. (5) and corresponds to a factor of 5 between the diffusion coefficient in

the silica-rich and silica poor composition. Fig. 9b shows diffusion profiles of wt.% MgO at $t = 0.1$ for $D_{\text{MgO}} = D_{\text{SiO}_2}$ and two different initial steps in wt.% MgO between 1% and 5% in one case and between 0.5% and 5% in a second case. Fig. 9c shows both the effect on the magnesium isotopic fractionation of the different contrasts in wt.% MgO and of three choices of β ($= 0.04, 0.05, \text{ and } 0.06$). The magnesium isotopic fractionation is seen to decrease as the ratio of the wt.% MgO between the interdiffusing melts decreases. Fig. 9c also shows that for a fixed difference in the wt.% MgO, the isotopic fractionation is proportional to β . Fig. 9d shows an assumed temperature profile across the model diffusion couple that is used to illustrate the effect of thermal diffusion on the magnesium concentration gradient at a no-flux boundary and on the shape of the magnesium isotopic profiles. Fig. 9e shows a distinct chemical gradient in magnesium at the boundary, which is exactly balanced by the thermal flux of magnesium to satisfy the no net flux boundary condition. Fig. 9f compares magnesium isotopic fractionation profiles with and without temperature differences

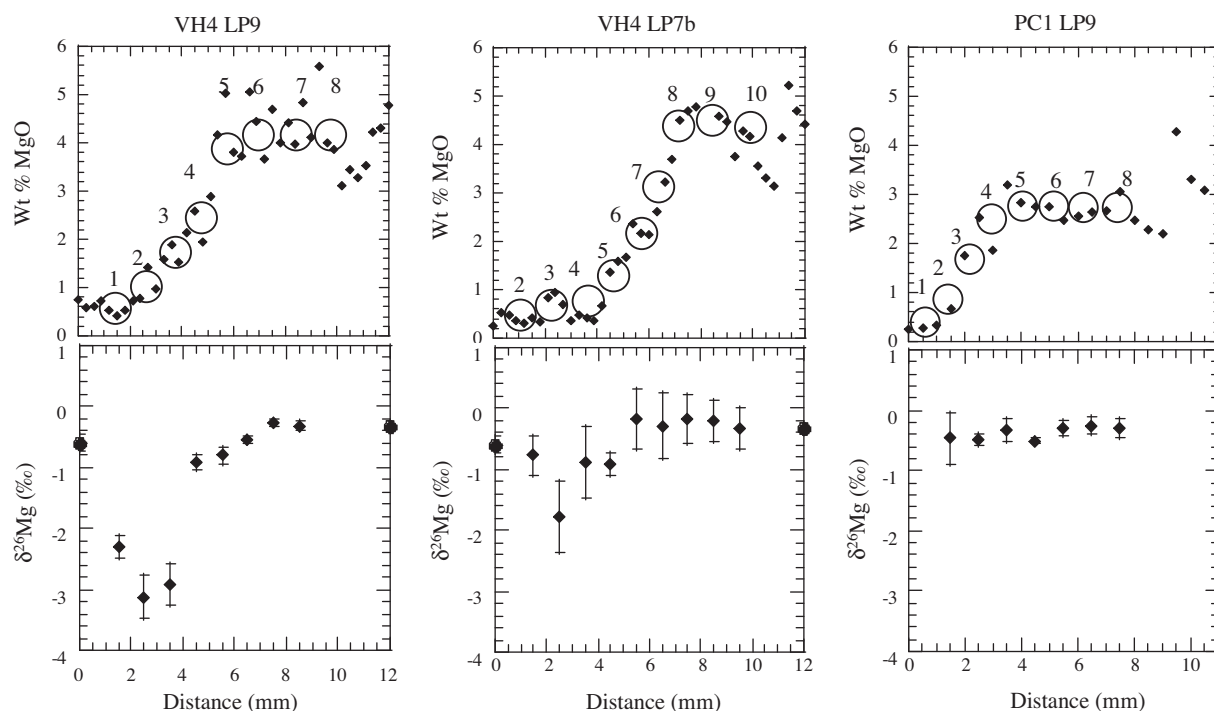


Fig. 8. The top row of panels show the magnesium concentration along traverses in the Vinal Cove samples LP9 and LP7b, and in sample PC1 LP9 from Aztec Wash. The large unfilled circles show the positions where 1 mm diameter drill holes were used to extract rock powders for magnesium isotopic analysis. The lower panels show the magnesium isotopic composition of the rock powders relative to the standard DSM3 (small diamonds with 95% CI error bars). The star symbols in the two Vinal Cove panels show the magnesium isotopic composition of felsic and mafic rock powders taken far from the contact.

at two different times. The effect of temperature on the isotopic fractionation is such that the heavy isotope ^{26}Mg is enriched at the two cold ends and that the effect penetrates in from the boundary. Because of the faster diffusion in the more mafic composition, the thermal fractionation affects a larger portion of the samples at the mafic end. The negative minimum in the magnesium isotopic profile in the vicinity of the interface is due to the faster chemical diffusion of ^{24}Mg from the more magnesium-rich to the less magnesium-rich side of the model diffusion couple. The effect of increasing time is to broaden but not significantly change the magnitude of the minimum. Note that at least for $t \leq 0.2$ the isotopic fractionations due to chemical diffusion and thermal diffusion affect different parts of the system and thus do not complicate extracting the separate kinetic isotope fractionation parameters β and β_T associated with chemical and thermal diffusion.

5.3. Thermo-chemical diffusion model calculations for the laboratory samples

Fig. 10 shows model fits to the magnesium concentration and isotopic data from laboratory diffusion couples GBM-1 and GBM-2. The magnesium isotopic composition of the powders that were used to make the diffusion couples is shown as black diamonds at the far right and left of the middle figures. The two bottom panels show the temperature profile assumed in the calculation when thermal diffusion is included in the calculation. The free parameters used to effect

the fits shown in Fig. 10 are the run time, the temperature profile, the composition dependence of the effective binary diffusion coefficients (given by α) and the chemical isotope fractionation factor β . The thermal fractionation factor $\beta_T = 0.58$ and the Soret coefficient ($\sigma_{\text{MgO}} = 1.7 \times 10^{-3}$) used in these calculations were taken from the earlier work by Richter et al. (2008) on thermal diffusion in molten basalt. The values of α and β that fit the data from GBM-1 and GBM-2 are similar to what Richter et al. (2008) reported ($\alpha = 12.5$, $\beta = 0.05$) for the magnesium concentration and isotopic fractionation in a rhyolite-basalt diffusion couple. Thermal fractionation results in the heavy isotopes becoming enriched at the colder parts of a temperature distribution, which is seen in Fig. 10 by the magnesium isotopic composition at the two ends of the diffusion couples being significantly elevated compared to the isotopic composition of the powders used to make the diffusion couples. The fit to the isotopic data in Fig. 10 could have been refined further by minor changes to the temperature profile, but given that the exact thermal parameters for our specific compositions are not independently known, and that the actual shape of the temperature profile within the sample is not directly measured, there seemed little merit in making further refinements. The important point was to show that reasonable temperature differences in the sample assembly (see Fig. 4) can explain the otherwise unexpected positive isotopic values at the ends of the diffusion couples.

The main reason for carrying out laboratory diffusion experiments juxtaposing rock powders from the natural

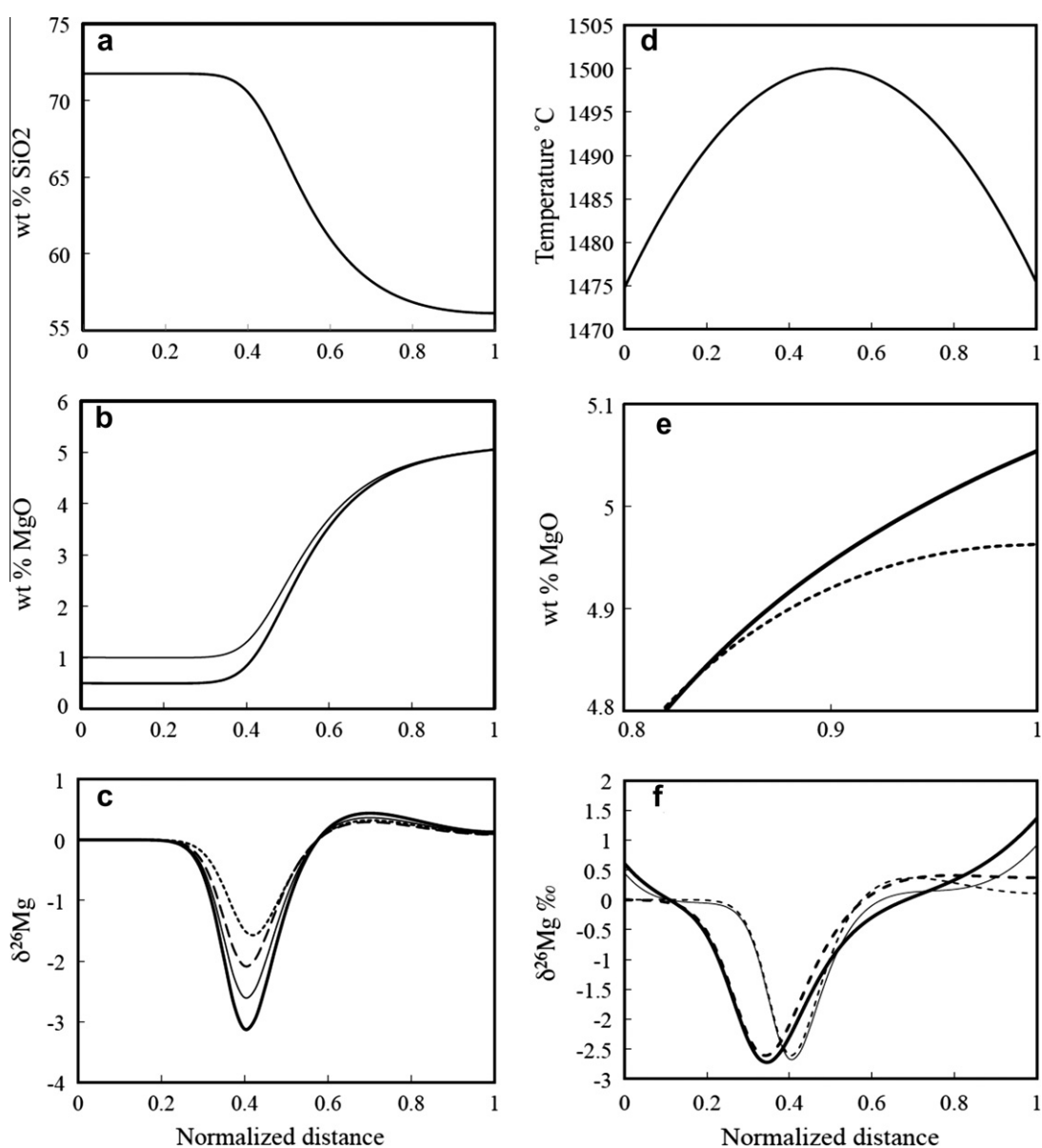


Fig. 9. The various panels in this figure show the results of idealized model calculations that illustrate the effect of diffusion coefficients depending on the SiO₂ concentration, of magnesium concentration differences, and the mass-dependence of magnesium isotope mobility as they affect isotope fractionation. The effect of temperature differences on the magnesium concentration profile and on the isotopic fractionation is also shown. Distance in these figures is measured in units of the dimension L , such that a normalized distance of one corresponds to a dimensional distance L . Time is measured in units of $t' = L^2/D$ where D is the effective binary diffusion coefficient (EBDC) of SiO₂ when SiO₂ = 52 wt.%. The EBDC for magnesium is assumed to be the same as that of silica and the compositional dependence of the diffusion coefficients is given by Eq. (5) with $\alpha = 10$. (a) Wt% SiO₂ at time $t' = 0.1$. (b) wt% MgO at $t' = 0.1$ for two choices of the concentration contrast. (c) Magnesium isotopic profiles from calculations with uniform temperature and MgO contrasts of a factor of 5 and $\beta = .05$ (short dashes) or 10 and three choices of the kinetic fractionation factor β (heavy line: $\beta = 0.06$, thin line: $\beta = 0.05$, and long dashes: $\beta = 0.04$). (d) Temperature profile assumed for illustrating thermal diffusion effects. (e) Profiles of wt.% MgO near the no-flux boundary at the mafic end of the model diffusion couple for an isothermal case (dashed line) and for a case (solid line) with temperature changing as shown in panel (d). (f) Magnesium isotope profiles with $\beta = 0.05$ for two isothermal cases (short dashes for $t' = 0.1$ and longer heavy dashes for $t' = 0.2$) and two cases with temperature varying as shown in panel (d) (thin line for $t' = 0.1$ and heavy line for $t' = 0.2$). The parameters used for specifying the thermal flux are those given by Richter et al. (2008) for magnesium ($\sigma = 1.7 \times 10^{-3}$ for the Soret coefficient and $\beta_T = 0.58$ for the thermal fractionation of isotopes).

system was to determine the chemical diffusion isotopic fractionation factor β , which as shown in Fig. 10, is determined by the isotopic fractionations in the vicinity of original interface and not significantly affected by thermal effects at the

boundaries. A value of $\beta \sim 0.045$ is a reasonable choice for comparing model calculations to the isotopic fractionations found in the traverses from Vinal Cove. $\beta = 0.045$ will also be used to model the data from Aztec Wash, but as will

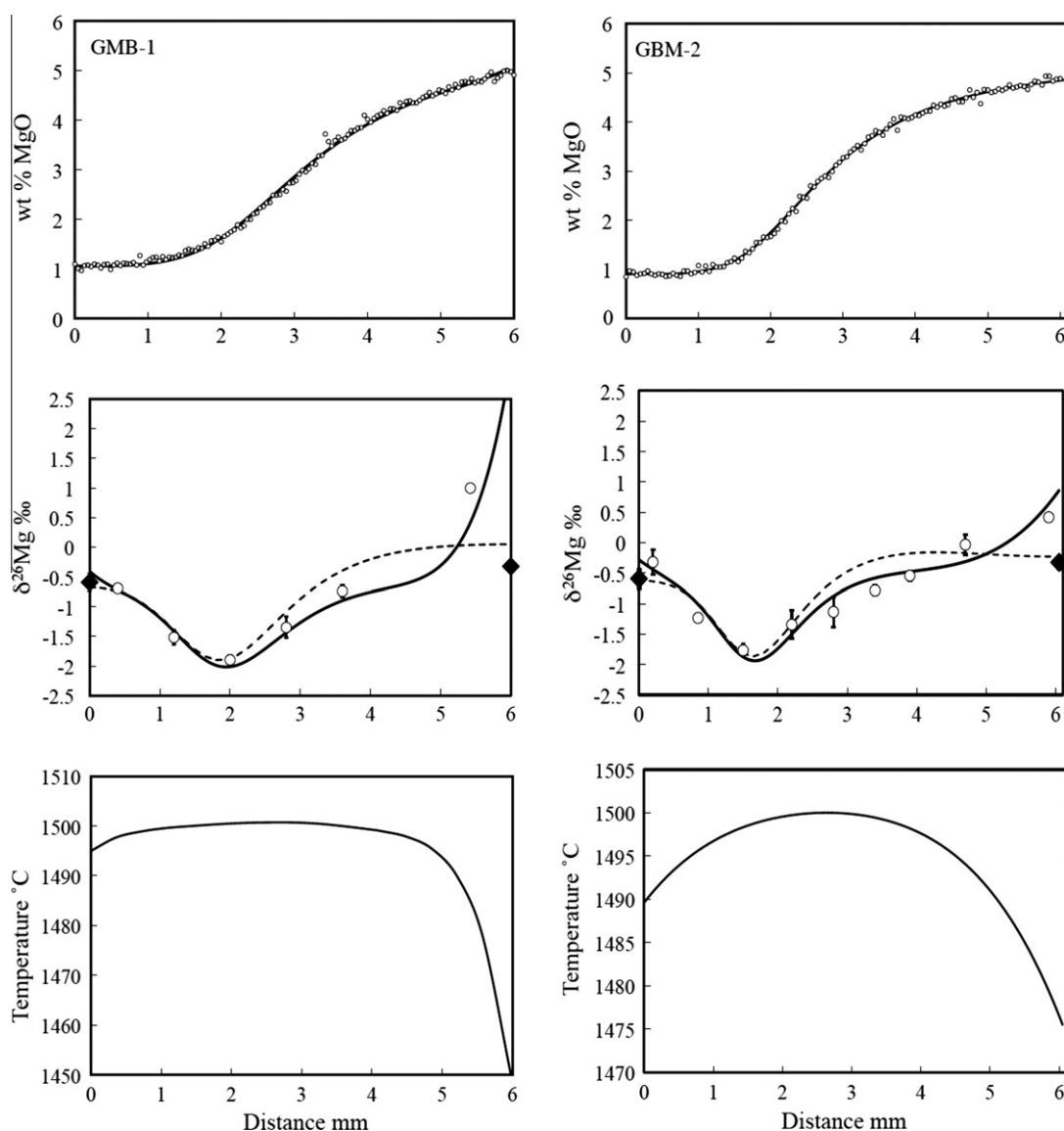


Fig. 10. Model calculations compared to the magnesium concentration and isotopic data from laboratory diffusion couples GBM-1 and GBM-2. The wt.% MgO of sample GBM-1 was fit as shown in the upper left panel with $D_{MgO} = D_{SiO_2}$ and the dependence of D_{MgO} and D_{SiO_2} on the local wt.% SiO_2 calculated using Eq. (5) with an exponent $\alpha = 10$. Thermal effects were calculated using a Soret coefficient $\sigma_{MgO} = 1.7 \times 10^{-3}$ taken from Richter et al. (2008). The non-dimensional time for the fit to the GBM-1 data is $t' = 0.069$ in units L^2/D_{SiO_2} where L is the length of the diffusion couple (6 mm) and D_{SiO_2} is the effective binary diffusion coefficient of silica when $SiO_2 = 52$ wt.% and $T = 1500$ °C. The middle panel compares the measured isotopic compositions from experiment GBM-1 (open circles) with magnesium isotopic profiles calculated for an isothermal case (dashed line) and one with the temperature distribution shown in the lower panel (solid line). The parameters used to model the mass dependence of the chemical diffusion and thermal diffusion of experiment GBM-1 are $\beta = 0.045$ and $\beta_T = 0.58$. The black diamonds at each end of the middle panel show the magnesium isotopic composition of the rock powders used to make the diffusion couple. The panels showing the results for GBM-2 are the same as those for GBM-1 except that the best fit was obtained at $t' = 0.05$ with $\beta = 0.04$ and the temperature distribution shown in the lower panel.

be seen below, the actual value of β used for this comparison is not important given that we did not find any significant isotopic fractionation in the Aztec Wash samples.

5.4. Chemical diffusion model calculations for the natural samples

In this section a magnesium isotopic fractionation parameter $\beta = 0.045$ is used to calculate the magnesium

isotopic fractionation along profiles VH4 LP9, VH4 LP7b from Vinal Cove and PC1 LP9 from Aztec Wash that would be expected if the mass transport implied by the magnesium concentration gradients were due to entirely chemical diffusion of magnesium.

5.4.1. Vinal Cove samples VH4 LP9 and VH4 LP7b

Fig. 11 shows the fit of model profiles to the magnesium concentration data and isotopic composition of transects

VH4 LP9 and VH4 PL7b from Vinal Cove. The only free parameter used in calculating the profiles is time. All other parameters ($\alpha = 10$, $\beta = 0.045$, $D_{\text{Mg}} = D_{\text{Si}}$) are taken to be the same parameters that were used to fit the data from the laboratory diffusion couple GBM-1. It was further assumed that thermal fractionations would have been negligible because the much faster diffusion of heat compared to chemistry would have eliminated any significant temperature differences on a time scale far too short for the chemistry to have been affected to any significant degree. Two model profiles are shown for the LP7b data to illustrate how different choices for the fit to the magnesium concentration data affects the calculated isotopic fractionation.

The length scale used to re-dimensionalize the calculated fit to the data from VH4 LP9 was 3 cm and for VH4 LP7b 1.5 cm. These length scales result in dimensional times of $t = 0.126/D_{\text{MgO}}$ for the fit to LP9 and $t = 0.039/D_{\text{MgO}}$ and $t = 0.063/D_{\text{MgO}}$ for the two fits to LP7b profiles. We can make a ‘back of the envelope’ estimate of time by assuming a fixed temperature of 1200 °C for the magmatic system, in which case $D_{\text{MgO}} \sim 2.5 \times 10^{-8} \text{ cm}^2/\text{s}$ and the dimensional time derived from the fit to the VH4 LP9 data is about 60 days.

5.4.2. Aztec Wash Sample PC1 LP9

Fig. 12 shows the fit of two model profiles to the magnesium concentration and isotopic data from transect PC1

LP9 from Aztec Wash. The magnesium concentration data are not adequate to constrain a specific calculated concentration profile and thus two choices are shown for non-dimensional profile times of 0.02 and 0.04. The parameters used for both cases are $\alpha = 10$, $\beta = 0.045$, and $D_{\text{MgO}} = D_{\text{SiO}_2}$. The temperature is assumed to have been sufficiently uniform that thermal fluxes are not included in the calculation.

6. SUMMARY AND DISCUSSION

The main goal of the present work was to determine the degree to which the kinetic isotope fractionations by chemical diffusion measured in laboratory experiments are also found in natural settings. For this purpose two experimental diffusion couples juxtaposing mafic and felsic composition melts made from rock powders sampled at Vinal Cove were used to determine the degree to which chemical diffusion of magnesium in this system would result in isotopic (Fig. 6). Model calculations were used to fit the elemental and isotopic data measured in glasses recovered from the diffusion experiments and in this way determine the effective binary diffusion coefficient (EBDC) of magnesium and how the EBDC depends on both silica content of the melt and on the mass of the individual magnesium isotopes. Because of the inevitable temperature gradients in the piston cylinder assembly used for annealing the diffusion couples (Fig. 4) the model calculations also included mass fluxes driven by

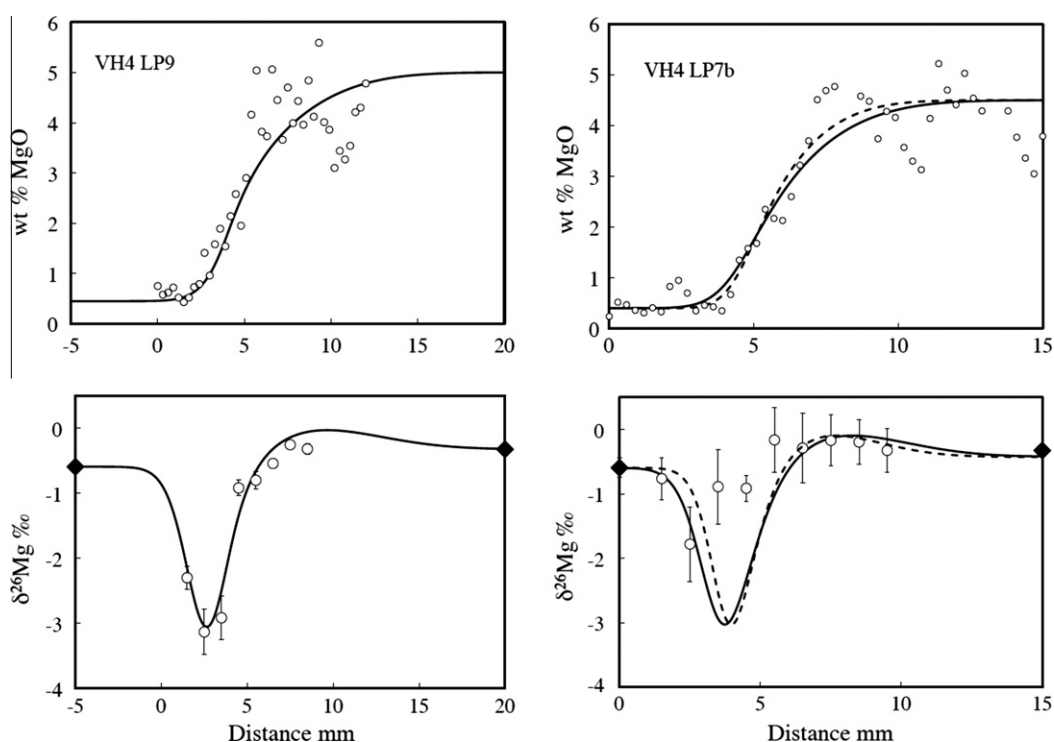


Fig. 11. Profiles from model calculations are compared to the magnesium concentration and isotopic data from profile LP9 (on the left) and LP7b (on the right) from Vinal Cove. The diamond symbols at each end of the lower panels show the magnesium isotopic composition of samples taken sufficiently far from the contact that they would not have been affected by mass transport across the contact between the mafic composition on the right and the more felsic composition on the left. The model calculations assumed $D_{\text{MgO}} = D_{\text{SiO}_2}$, $\alpha = 10$, $\beta = 0.045$, and that thermal diffusion effects were negligible. The profiles that fit the LP9 data are from a calculation run to a non-dimensional time $t' = 0.014$. The two model cases shown for LP7b correspond to $t' = 0.0175$ (dashed line) and $t' = 0.028$ (continuous line).

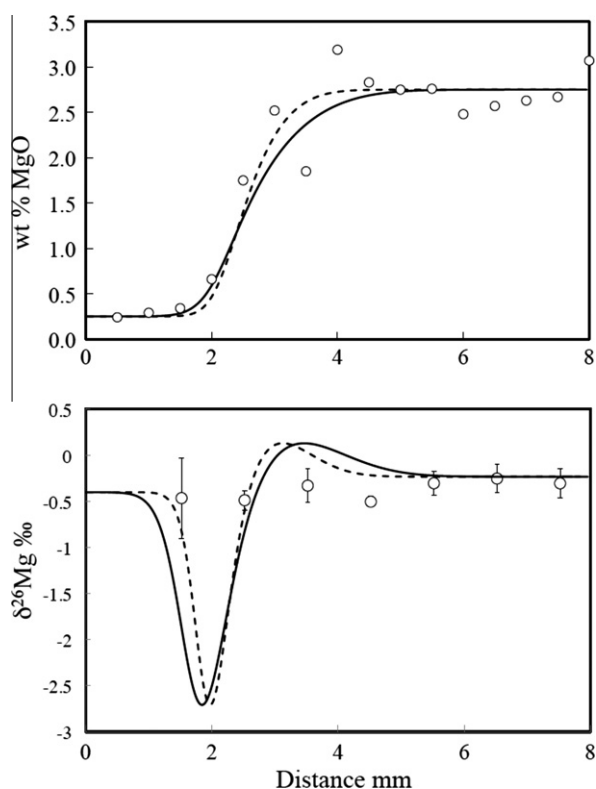


Fig. 12. Comparison between data from transect PC1 PL9 from Aztec Wash and profiles from model calculations of wt.% MgO and $\delta^{26}\text{Mg} \text{ ‰}$ using $D_{\text{MgO}} = D_{\text{SiO}_2}$, $\alpha = 10$, $\beta = 0.045$ for two nondimensional times of $t' = 0.02$ (dashed lines) and $t' = 0.04$ (solid lines).

temperature gradients (i.e., Soret diffusion). The results of idealized models were used to illustrate the effect of the various governing parameters on the elemental and isotopic profiles (Fig. 9). The chemical diffusion parameters derived from the model calculation fits to the laboratory data from couples GBM-1 and GBM-2 are summarized in Table 2. The estimates of the effective binary diffusion coefficients (EBDC) of MgO listed in Table 2 are for a melt with 52 wt.% SiO₂ at 1500 °C. The parameter α was used to specify the sensitivity of the EBDC to changes in the SiO₂ content of the melt as given by Eq. (5) and β was used to specify the relative value of the EBDC of the magnesium isotopes that results in the measured isotopic fractionations. The thermal effects were modeled using a Soret coefficient $\sigma_{\text{MgO}} = 1.7 \times 10^{-3}$ and a thermal isotope fractionation exponent $\beta_T = 0.58$ taken from the earlier work by Richter et al. (2008) on molten basalt. The effective binary diffusion coefficients for magnesium listed in Table 2 and it's

dependence on the wt.% SiO₂ of the liquid are reasonably similar to previously reported values by Richter et al. (2003) for a mid ocean ridge basalt ($D_{\text{MgO}} = 8 \times 10^{-7} \text{ cm}^2/\text{s}$ at 1450 °C for SUNY MORB with ~50 wt.% SiO₂ and $\alpha = 12$). The value of β that best fit the magnesium isotopic fractionation from couples GBM-1 ($\beta = 0.045$) and GBM-2 ($\beta = 0.04$) is also not significantly different from that reported by Richter et al. (2008) for a rhyolite-basalt interdiffusion experiment ($\beta = 0.05 \pm 0.005$).

Major element concentrations and magnesium isotopic compositions were measured across two mafic to felsic contacts at Vinal Cove in the Vinalhaven igneous complex in Maine and one similar contact in the Aztec Wash pluton in Nevada. Model calculations were used to fit the changes in MgO in the vicinity of the contact and then to compare the measured magnesium isotopic variations to what would be expected based on laboratory-derived parameters for the kinetic isotope fractionation due to molecular diffusion (Figs. 11 and 12). In the case of profile VH4 LP9 the calculated isotope profile is an almost perfect match to the measured values, which we take as strong evidence that at this location the transport of magnesium was effectively entirely by diffusion. An important result from our study is that the same isotopic fractionation associated with chemical diffusion determined in highly controlled laboratory experiments can also be found in a natural setting. Also important is that we did not find a similarly good match between calculated and observed magnesium isotopic fractionations in the case of data from VH4 LP7b. While there is some variation of the magnesium isotopes at VH4 LP7b, the magnitude and spatial distribution is not what one expects if the transport of magnesium indicated by the concentration gradients were due entirely to diffusion. We interpret this to mean that some other mechanism, most likely mixing, played an important role in the transport of magnesium. The sort of mixing we have in mind is the result of fluid flow causing melts of different composition to be mixed in different proportions into particular volumes thus giving rise to concentration differences among these particular volumes. If the mixing would have been on a sufficiently small scale, diffusion would have had ample time to erase any isotopic variations that would have arisen in the earliest stages of diffusive exchange. The important point illustrated by the data from VH4 LP7b is that the existence of elemental gradients is not in itself sufficient to show that chemical diffusion was the responsible transport mechanism. It follows that the extent of a chemical gradient should not be used as a measure of time unless there is independent evidence that the gradient was in fact produced by molecular diffusion. It is our contention that kinetic isotope fractionations provide the key data for establishing whether or not

Table 2

Parameters used to fit the chemical diffusion of magnesium and associated isotopic fractionation in experiments juxtaposing melts made from mafic and felsic rock powders sampled at Vinal Cove sufficiently far from the contact so that they would not have been affected by diffusion across the contact.

Sample	t in units $L^2/D_{\text{SiO}_2=0.52}$	Run time hours	$\beta : \frac{D_{26\text{Mg}}}{D_{24\text{Mg}}} = \left(\frac{24}{26}\right)^\beta$	α_{MgO}	$D_{o,\text{MgO}}(\text{cm}^2/\text{s})$
GBM-1	0.069	22.5	0.045	10	3.1×10^{-7}
GBM-2	0.05	10.0	0.040	10	5.0×10^{-7}

molecular diffusion was the process responsible for an observed elemental gradient in a natural setting.

The situation in sample PC1 LP9 from Aztec Wash is less clear than for the two Vinal Cove samples. The correlated composition changes in MgO, CaO, and FeO across the contact between mafic and felsic rocks (Fig. 7) seem to suggest mass transport in a thin boundary layer. However this boundary layer is sufficiently thin that a case could be made that the sampling for the isotopic measurements was too widely spaced to resolve any expected negative $\delta^{26}\text{Mg}$ values due to chemical diffusion (Fig. 12). On the other hand, the measured isotopic compositions do not show the expected positive $\delta^{26}\text{Mg}$ values in the mafic side of the contact, which suggests that chemical diffusion was not the dominant transport mechanism. The only firm conclusion that we can draw based on the data at PC1 LP9 is that the system had to have cooled very quickly, which is consistent with the interpretation discussed in section 5.2 that at Aztec Wash thin mafic sheets spread as lava flows on the effective base of the granitic magma chamber, quenching against the cooler substrate of crystals accumulated from the overlying granitic magma.

Our interpretation that the mass transport mechanism between mafic and felsic melts at Vinal Cove changed from chemical diffusion (along VH4 LP9 to mechanical mixing dominated (along VH4 LP7b) over a distance of a few centimeters is a first sight quite surprising. On reflection, the interpretation that there would have been mechanical mixing due to the relative motions of the two melts is less surprising to us than to have found a case where the transport appears to have been entirely by diffusion. For the transport to have been entirely by molecular diffusion, the relative flow of the melts must have very rapidly become negligible or perfectly laminar and parallel to the contact.

Because of the correspondence between the magnesium isotopic fractionation measured in sample VH4 PL9 and what is calculated using experimentally determined kinetic isotope fractionation parameters we are quite confident that the magnesium diffusion profile at this location can be used to constrain the local cooling rate. The fit to the VH4 LP9 data shown in Fig. 11 resulted in an estimate of time $t' = 0.014$ measured in units of $L^2/D_{\text{MgO}(X_{\text{SiO}_2}=0.52)}$. This is the time that would be required to fit the data if the diffusion rate of magnesium were unchanging with time and then suddenly stopped. However in a system cooling at a finite rate one needs to take into account that the diffusivity will decrease as the temperature decreases, which we can write as $D_{(t)} = \hat{D}e^{-E_a/RT(t)}$ where \hat{D} is the frequency factor (cm^2/s), E_a is the activation energy (in J/mol), T is the absolute temperature and R is the universal gas constant (8.3145 J/K mol). For present purposes we will assume an activation energy of 200 kJ/mol based on the results of experiments by Liang and Davis (2002) that determined an activation energy between 192 and 217 kJ/mol for diffusion in a haplobasalt. Using this activation energy together with an estimate of $D_{\text{MgO}(X_{\text{SiO}_2}=0.52)} = 4 \times 10^{-7} \text{ cm}^2/\text{s}$ at $T = 1773 \text{ K}$ (the average of the two estimates given in Table 2) results in a frequency factor of $\hat{D} = 0.31$. The initial temperature of the mafic magma from Vinal Cove is estimated to be approximately 1473 K based on the liquidus

temperature calculated using MELTS (Ghiorso and Sack, 1995; Asimow and Ghiorso, 1998) for the average mafic composition of sample VH4, $P = 1 \text{ kbar}$, oxygen fugacity corresponding to the FMQ (fayalite-magnetite-quartz) buffer, and relatively dry conditions (water $< 1 \text{ wt.}\%$). Thus the time evolution of the diffusivity of magnesium due to cooling at Vinal Cove can be written as

$$f(t) = e^{(E_a/R)[1/1473 - 1/T(t)]} \quad (6)$$

where $f(t)$ is the factor by which the diffusion of magnesium declines with time due to cooling from $T = 1473 \text{ K}$. The value of $t = 0.014$ given in connection with the fit shown in Fig. 11 represents the nondimensional time it takes to fit the data from VH4 LP9 when of the diffusivities do not change other than due to the evolving silica distribution. When the diffusivities are declining with time at a finite rate due to cooling, the cooling rate becomes the parameter that determines the fit to the data. The constraint on the cooling rate at VH4 LP9 is given by the integral (see discussion in Crank, 1975 regarding time dependent diffusion).

$$\int_0^\infty f(\tau) d\tau = 0.014 \quad (7)$$

In practice the integral only has to be evaluated up to a time where the diffusivity has become so small as to have negligible effect on any further mass transport. In the case of an exponentially decaying temperature $T_{(t)} = 1473 e^{-\lambda t}$, the decay constant that satisfies the integral is $\lambda = 4.4$ measured in units of $D_{\text{MgO}(X_{\text{SiO}_2}=0.52)}/L^2$. In dimensional terms this corresponds to a cooling of 300 K in 1.9×10^7 seconds (~ 220 days) for $L^2/D_{\text{MgO}(X_{\text{SiO}_2}=0.52)} = 3.6 \times 10^8$ seconds corresponding to $L = 3 \text{ cm}$ and $D_{\text{MgO}(X_{\text{SiO}_2}=0.52)} = 2.5 \times 10^{-8}$. This value of $D_{\text{MgO}(X_{\text{SiO}_2}=0.52)}$ is the average D_{Mgo} from Table 2 reduced from $T = 1773 \text{ K}$ to 1473 K using an activation energy of 200 kJ/mole.

Our estimate that the site of sample VH4 LP9 cooled by 300 °C in about 220 days is surprisingly fast. This cooling rate is not local in the sense of being due to heat transport across the contact between melt with initially different temperatures. The initially cold side of the contact (presumably the felsic side) would be heating up while the hot side would cool. The time it would take for the temperature within one centimeter of the interface to change from an initial contrast $T_o \pm \Delta T$ to $T_o \pm 0.1\Delta T$ can be estimated using the error function solution $T_{(eta)} = T_o \pm \Delta T_o \text{erf}(\eta)$ where $\eta = l/\sqrt{\kappa t}$, l is distance from the interface, κ is the thermal diffusivity and t is time. The temperature contrast is thus reduced to 10% when $\text{erf}(\eta) = 0.1$, which corresponds to $\eta \sim 0.1$. At a distance of one centimeter from the boundary, $\eta \rightarrow 0.1$ in about 250 s for an assumed value of $\kappa \sim 0.01 \text{ cm}^2/\text{s}$. In making this estimate latent heat is ignored, but even if it were included in calculating cooling times, the general conclusion would be much the same – the temperature differences within one centimeter of the contact where we found chemical gradients will have become very small in a matter of minutes. This indicates that the cooling rate of about a 1.5 °C per day inferred from the chemical gradients at VH4 LP9 must refer to cooling on some larger scale. We can at the other extreme compare our inferred cooling rate with the large-scale cooling of a

magmatic system such as a lava lake. The cooling rate measured at Kilauea Iki lava lake is only as fast as hundred degrees in about 100 days in the upper few meters below the surface (Rosalind L. Helz, personal communication). Below ten meters in the lava lake the temperature did not begin to cool for several years. Another way to illustrate the implications of the cooling rate inferred for site VH4 is to consider that the center of a slab of thickness $2L$ cools by 50% of its temperature contrast with its surroundings when $\kappa t/L^2 \sim 0.4$ (Fig. 11 in Chapter III of Carslaw and Jaeger, 1959). For 50% cooling, which would have certainly quenched the diffusion profile, to take place on a time scale of order 10^7 seconds, the slab would have to be only 10 meters in thickness. Given the somewhat surprising conclusion that the location we sampled at VH4 just happened to have been very close to a chilled margin, we should at least consider alternative interpretations of the thermal history inferred from the magnesium profiles in sample VH4 LP9.

The key assumption that the mass transport at VH4 LP9 was by diffusion is hard to challenge because of the virtually perfect correspondence between the magnesium elemental gradient and the magnesium isotopic fractionation. Could we have made a mistake in our choice of the value for the diffusion coefficient? The value for $D_{\text{MgO}}(X_{\text{SiO}_2}=0.52)$ used above to calculate dimensional time was derived from experimental diffusion couples made from rock powders from Vinal Cove. These powders were nominally dry, whereas the natural system might have had significant amounts of water. But the effect of water would be to increase the diffusivity of magnesium and thus the required cooling rate would have been even faster than we estimated for a dry system. One other consideration is that we have implicitly assumed that the diffusive exchange of magnesium at VH4 LP9 was in melts. If the diffusion took place after the system had solidified, diffusion in the minerals would have been very much slower than in melts and thus a much longer cooling time would be able to account for the magnesium data. It seems that the data from VH4 LP7b provides evidence that the mass transport of magnesium did not take place after the system solidified. Once the system solidified, diffusion would have been the only mass transport mechanism and thus both LP9 and LP7b would be expected to have similar magnesium isotopic fractionation profiles. The fact that there is evidence of magnesium transport at LP7b but not the expected isotopic fractionation implies that the transport could not have occurred after the system solidified. The most straightforward conclusion seems to be that the transport of magnesium in the places we sampled took place while the system was mostly molten and thus the rapid cooling of about $1.5^\circ\text{C}/\text{day}$ inferred from the data at VH4 LP9 is likely to be correct. This seems to imply proximity to a cold boundary. It could be that the rapid cooling we infer was due to hydrothermal transport of heat, but field and petrographic observations emphasizing the overall scarcity of hornblende would seem to rule out large amounts of water having been involved at Vinal Cove (see Wiebe et al., 2004 for details).

In closing we want to emphasize the key role of the isotopic data in the overall structure of our arguments. The magnesium isotopic data was critical for establishing that

the mass transport mechanism at VH4 LP9 was chemical diffusion and thus that the extent of the transport could be used to make inferences regarding the thermal history. A specific interpretation of the very rapid cooling rate that we inferred for sample VH4 LP9 will require further fieldwork and isotopic analyses of additional samples. The fact that a very similar magnesium concentration gradient was found at the nearby location VH4 LP7b but that the magnesium isotopic fractionation was not consistent with chemical diffusion was interpreted to mean that some transport process besides chemical diffusion played a significant role there. Furthermore, the difference between the isotopic fractionation along LP9 and LP7b profiles was used to argue that the transport of magnesium must have taken place while the systems were still molten to a high degree. The key point is that the isotopic data, both when it shows the expected fractionation by diffusion and when it does not, provide important insight into the transport processes and time scales in a system where melts of different composition interacted.

ACKNOWLEDGEMENTS

The work reported here is part of a larger study that constituted Rahul Chopra's PhD dissertation (2010, Department of the Geophysical Sciences at the University of Chicago). Rahul Chopra would like to acknowledge Robert Wiebe, Guilherme Gualda, and Calvin Miller for introducing him to the field localities of this study and Paul Craddock for assistance with the isotopic analyses. The work was supported by a DOE grant DE-FG02-01ER15254,A005 to Frank Richter and NSF grant EAR-0337481 to E. Bruce Watson.

REFERENCES

- Asimow P. D. and Ghiorso M. S. (1998) Algorithmic modifications extending MELTS to calculate subsolidus phase relations. *Am. Mineral.* **83**, 1127–1131.
- Chakrabarti R. and Jacobsen S. B. (2010) The isotopic composition of magnesium in the inner Solar System. *Earth Planet. Sci. Lett.* **293**, 349–358.
- Carslaw H. S. and Jaeger J. C. (1959) *Conduction of Heat in Solids*, 2nd ed. Oxford University Press, Oxford.
- Crank J. (1975) *The Mathematics of Diffusion*, 2nd. Oxford University Press, Oxford.
- Dauphas N., Pourmand A. and Teng F.-Z. (2009) Routine isotopic analysis of iron by HR-MC-ICPMS: how precise and how accurate? *Chem. Geol.* **267**(3–4), 175–184.
- Falkner C. M., Miller C. F., Wooden J. L. and Heizler M. T. (1995) Petrogenesis and tectonic significance of the calc-alkaline, bimodal Aztec Wash pluton, Eldorado Mountains, Colorado River extensional corridor. *J. Geophys. Res.* **100**, 10453–10476.
- Galy A., Yoffe O., Janney P., Williams R., Cloquet C., Alard O., Halicz L., Wadhwa M., Hutcheon I., Ramon E. and Carignan J. (2003) Magnesium isotope heterogeneity of the isotopic standard SRM980 and new reference materials for magnesium-isotope ratio measurements. *J. Anal. At. Spectrom.* **18**, 1352–1356.
- Ghiorso M. S. and Sack R. O. (1995) Chemical mass transfer in magmatic processes. IV. A revised and internally consistent thermodynamic model for the interpolation and extrapolation of liquid-solid equilibria in magmatic systems at elevated temperatures and pressures. *Contrib. Miner. Petrol.* **119**, 197–212.

- Handler M. R., Baker J. A., Schiller M., Bennett V. C. and Yaxley G. M. (2009) Magnesium stable isotope composition of Earth's upper mantle. *Earth Planet. Sci. Lett.* **282**, 306–313.
- Harper B. E., Miller C. F., Koteas G. C., Cates N. L., Wiebe R. A., Lazzareschi D. S. and Cribb J. W. (2004) Granites, dynamic magma chamber processes and pluton construction: the Aztec Wash pluton, Eldorado Mountains, Nevada, USA. *Trans. Earth Sci.* **95**, 277–296.
- Hawkins D. P., Wobus R. A. and Wiebe R. A. (2002) Silurian U–Pb zircon dates from the Vinalhaven intrusion and associated volcanic rocks, Penobscot Bay, Maine. *Geol. Soc. Am.* **34**(6), 42 (Abstracts with Programs).
- Hogan J. P. and Sinha A. K. (1989). Compositional variation of plutonism in the coastal Maine magmatic province: mode of origin and tectonic setting. In *Igneous and Metamorphic Geology, Maine Geological Survey, Department of Conservation, Studies of Maine Geology* (eds. R. D. Tucker and R. G. Marvinney) **4**, pp. 1–33.
- Huang F., Glessner J., Ianno A., Lundstrom C. and Zhang Z. (2009) Magnesium isotopic composition of igneous rock standards measured by MC-ICP-MS. *Chem. Geol.* **268**, 15–23.
- Leshner C. E. and Walker D. (1986) Solution properties of silicate liquids from thermal diffusion experiments. *Geochim. Cosmochim. Acta* **50**, 1397–1411.
- Li W.-Y., Teng F.-Z., Ke S., Rudnick R. L., Gao S., Wu F.-Y. and Chappell B. W. (2010) Heterogeneous magnesium isotopic composition of the upper continental crust. *Geochim. Cosmochim. Acta* **74**, 6867–6884.
- Liang Y. and Davis A. M. (2002) Energetics of multicomponent diffusion in molten CaO–Al₂O₃–SiO₂. *Geochim. Cosmochim. Acta* **66**, 635–646.
- Liu S.-A., Teng F.-Z., He Y.-S., Ke S. and Li S.-G. (2010) Investigation of magnesium isotope fractionation during granite differentiation: implication for Mg isotopic composition of the continental crust. *Earth Planet. Sci. Lett.* **297**, 646–654.
- Lundstrom C. C., Chaussidon M., Hsui A. T., Kelemen P. and Zimmerman M. (2005) Observations of Li isotopic variations in the Trinity Ophiolite: evidence for isotopic fractionation by diffusion during mantle melting. *Geochim. Cosmochim. Acta* **69**(3), 735–751.
- Miller C. F., Miller J. S. and Faulds J. E. (2005) Miocene volcano-plutonic systems, southern Nevada: a window into upper crustal magmatic processes. In: *Western Great Basin Geology: Fieldtrip Guidebook and Volume*. (eds. C. Stevens and C. Cooper), GSA Cordilleran Section, **99**, pp. 37–66.
- Miller C. F., Furbish D. J., Walker B. A., Claiborne L. L., Koteas G. C., Bleick H. A. and Miller J. S. (2011) Growth of plutons by incremental emplacement of sheets in crystal-rich host: Evidence from Miocene intrusions of the Colorado River region, Nevada, USA. *Tectonophysics* **500**, 65–77.
- Patrick D. W. and Miller C. F. (1997) Processes in a composite, recharging magma chamber: evidence from magmatic structures in the Aztec Wash pluton, Nevada. *Proceedings of the 30th International Geological Congress* **15**, 121–135.
- Richter F. M., Liang Y. and Davis A. M. (1999) Isotope fractionation by diffusion in molten oxides. *Geochim. Cosmochim. Acta* **63**, 2853–2861.
- Richter F. M., Davis A. M., DePaolo D. J. and Watson E. B. (2003) Isotope fractionation by chemical diffusion between molten basalt and rhyolite. *Geochim. Cosmochim. Acta* **67**, 3905–3923.
- Richter F. M., Watson E. B., Mendybaev R. A., Teng F.-Z. and Janney P. E. (2008) Magnesium isotope fractionation in silicate melts by chemical and thermal diffusion. *Geochim. Cosmochim. Acta* **72**, 206–220.
- Richter F. M., Watson E. B., Mendybaev R. A., Dauphas N., Georg B., Watkins J. and Valley J. (2009) Isotopic fractionation of the major elements of molten basalt by chemical and thermal diffusion. *Geochim. Cosmochim. Acta* **73**, 4250–4263.
- Teng F.-Z., McDonough W. F., Rudnick R. L. and Walker R. J. (2006) Diffusion-driven extreme lithium isotopic fractionation in country rocks of the Tin Mountain pegmatite. *Earth Planet. Sci. Lett.* **243**, 701–710.
- Teng F.-Z., Wadhwa M. and Helz R. T. (2007) Investigation of magnesium isotope fractionation during basalt differentiation: Implications for a chondritic composition of the terrestrial mantle. *Earth Planet. Sci. Lett.* **261**, 84–92.
- Teng F. Z., Li W., Ke S., Marty B., Dauphas N., Huang S., Wu F. and Pourmard A. (2010) Magnesium isotopic composition of the Earth and chondrites. *Geochim. Cosmochim. Acta* **74**, 4150–4166.
- Watkins J. M., DePaolo D. J., Huber C. and Ryerson F. J. (2009) Liquid composition-dependence of calcium isotope fractionation during diffusion in molten silicates. *Geochim. Cosmochim. Acta* **73**, 7341–7359.
- Watson E. B., Wark D. A., Price J. D. and Van Orman J. A. (2002) Mapping the thermal structure of solid-media pressure assemblies. *Contrib. Miner. Petrol.* **142**, 640–652.
- Wiebe R. A., Frey H. and Hawkins D. P. (2001) Basaltic pillows mounds in the Vinalhaven intrusion, Maine. *J. Volcanol. Geoth. Res.* **107**, 171–184.
- Wiebe R. A. and Hawkins D. P. (2003) Construction of the Vinalhaven intrusive complex, Vinalhaven Island, coastal Maine. *Geol. Soc. Am.* **35**(3), 36 (Abstracts with Programs).
- Wiebe R. A., Manon M. R., Hawkins D. P. and McDonough W. F. (2004) Late-stage mafic injection and thermal rejuvenation of the Vinalhaven granite, coastal Maine. *J. Petrol.* **45**(11), 2133–2153.
- Young E. D., Tonui E., Manning C. E., Schauble E. and Macris C. A. (2009) Spinel–olivine magnesium isotope thermometry in the mantle and implications for the Mg isotopic composition of Earth. *Earth Planet. Sci. Lett.* **288**, 524–533.

Associate editor: Clark M. Johnson